

Perpendicular magnetic anisotropy of Ir/CoFeB/MgO trilayer system tuned by electric fields

Witold Skowroński^{1,2*}, Takayuki Nozaki¹, Yoichi Shiota¹, Shingo Tamaru¹, Kay Yakushiji¹, Hitoshi Kubota¹, Akio Fukushima¹, Shinji Yuasa¹, and Yoshishige Suzuki^{1,3}

¹Spintronics Research Center, National Institute of Advanced Industrial Science and Technology, Tsukuba, Ibaraki 305-8568, Japan

²Department of Electronics, AGH University of Science and Technology, Al. Mickiewicza 30, 30-059 Kraków, Poland

³Graduate School of Engineering Science, Osaka University, Toyonaka, Osaka 560-8531, Japan

E-mail: skowron@agh.edu.pl

Received February 3, 2015; accepted April 7, 2015; published online April 24, 2015

The perpendicular magnetic anisotropy of an Ir/CoFeB/MgO trilayer was investigated after annealing at temperatures ranging from 200 to 350 °C. In the trilayer system annealed at 300 °C, we measured an interface anisotropy energy of 1.9 mJ/m². Further annealing led to mixing of the buffer and ferromagnet, degrading the properties of the latter. In addition, we show the dependence of the magnetic anisotropy on the bias voltage. The presented system is important for the development of perpendicular magnetic tunnel junctions for storage applications.

© 2015 The Japan Society of Applied Physics

Magnetic multilayers are one of the most attractive systems for digital storage applications.¹⁾ Current magnetic random-access memory (MRAM) scalability issues can be overcome by the use of materials with perpendicular magnetic anisotropy (PMA).^{2,3)} Systems with PMA take advantage of either volume anisotropy properties, as in, for example, Fe-based alloys,⁴⁾ or anisotropy at an interface between Co and a heavy metal⁵⁾ or between Fe and CoFe alloys and MgO.^{6–8)} Recently, numerous groups have also studied the effect of a capping or underlayer material on PMA.^{9–15)} In addition to the broadly investigated PMA in these systems, the tunability of the PMA energy using an applied bias voltage is an interesting alternative for controlling the thin film magnetization.^{16–18)}

It has already been demonstrated that the critical switching current can be reduced while maintaining high thermal stability of the storage layer in a magnetic tunnel junction (MTJ).³⁾ However, to fulfill the requirements for a 30-nm-scale memory cell, the product of the effective PMA energy density and the storage layer thickness should exceed $K_{\text{eff}}t > 0.4\text{--}0.6\text{ mJ/m}^2$.¹⁹⁾ Further increases in the PMA and preservation of the structure that exhibits high tunneling magnetoresistance (TMR) and low switching current require alternative storage layer systems. One possibility involves a double CoFeB/MgO interface.^{20,21)} Alternatively, theoretical calculations for an Ir/Fe bilayer predict very high PMA values,²²⁾ however, contradictory reports also exist.²³⁾

In this Letter, we experimentally investigate the use of an Ir buffer in a CoFeB storage layer application, which exhibits higher PMA energy than any other metal/CoFeB bilayer. We note that comparably high PMA values were also measured in single-crystal Fe/MgO/Fe MTJs deposited by molecular beam epitaxy (MBE)^{24–26)} on a Cr or MgO buffer; however, for practical applications, the sputtering deposition method investigated in this paper is more relevant. Additionally, we investigate PMA control using an electric field, which could further reduce the power consumption of prototype devices based on the presented technology.

For the experiment, we used the following multilayer structure (thicknesses in nm): Ta (5)/Ir (5)/CoFeB (t_{CoFeB})/MgO (2.5)/CoFeB (5)/Ta (5)/Ru (5)/Pt (2), which was deposited on a chemical–mechanical-polished Si substrate, with t_{CoFeB} values ranging from 0.7 to 4 nm. The Ir layer was deposited on a room-temperature stage at the process gas pressure of $P_p = 0.05\text{--}0.1\text{ Pa}$. The base pressure of the

sputtering apparatus was $P_b = 5 \times 10^{-7}\text{ Pa}$. The MTJs were fabricated into rectangular devices with dimensions of 2 and 6 μm using optical lithography, ion-beam milling, and lift-off processes. The thickness of the $(\text{Co}_{15}\text{Fe}_{85})_{80}\text{B}_{20}$ was chosen so that the thick upper CoFeB layer is always in-plane magnetized, whereas the bottom layer's effective anisotropy changes from in-plane to perpendicular with changes in the thickness or annealing temperature. This crossed magnetic anisotropy alignment enabled us to calculate the magnetic anisotropy surface energy on the basis of the magnetization versus the magnetic field dependence, which was calculated from a resistance measurement based on a model presented in Ref. 27. A thick MgO tunnel barrier ensured a high resistance–area product of about 100 $\text{k}\Omega\text{-}\mu\text{m}^2$; therefore, we could neglect the effect of the small resistance of the electrical connections, as well as any current-related phenomena such as the spin-transfer torque or Oersted field, on our results. After microfabrication, samples were successively measured in a room-temperature probe station with magnetic field values of up to 2 T and annealed in a vacuum furnace at temperatures ranging from 200 to 350 °C for 1 h followed by cooling for 2 h. We note that the as-deposited samples were unintentionally annealed at 170 °C for 2 min during the microfabrication process. The magnetic properties were measured in a vibrating sample magnetometer (VSM) using unpatterned films with only the bottom CoFeB layer present, which were annealed under the same conditions as the patterned devices. High-frequency measurements were performed using a custom-designed radio-frequency (RF) two-axis rotating probe, which enables magnetic field application at any polar or azimuthal angle. Instead of using an amplitude-modulated RF stimulus signal, we took advantage of additional coils placed inside the electromagnet, which are supplied with a low-frequency current, and thus performed field-modulated electric-field ferromagnetic resonance (FMR);²⁸⁾ this increased the sensitivity of our setup. Throughout this Letter, a positive bias voltage indicates electron accumulation in thin CoFeB/MgO interface.

We begin our discussion by presenting the magnetic properties of unpatterned films with various t_{CoFeB} values. The saturation magnetization (M_s) at different annealing temperatures is presented in Fig. 1(b). $\mu_0 M_s$ remains equal to 1.65 T for annealing temperatures up to 300 °C; however, a slight decline is visible at $t_{\text{CoFeB}} < 1\text{ nm}$ owing to mixing with the Ir buffer layer. The product of t_{CoFeB} and the

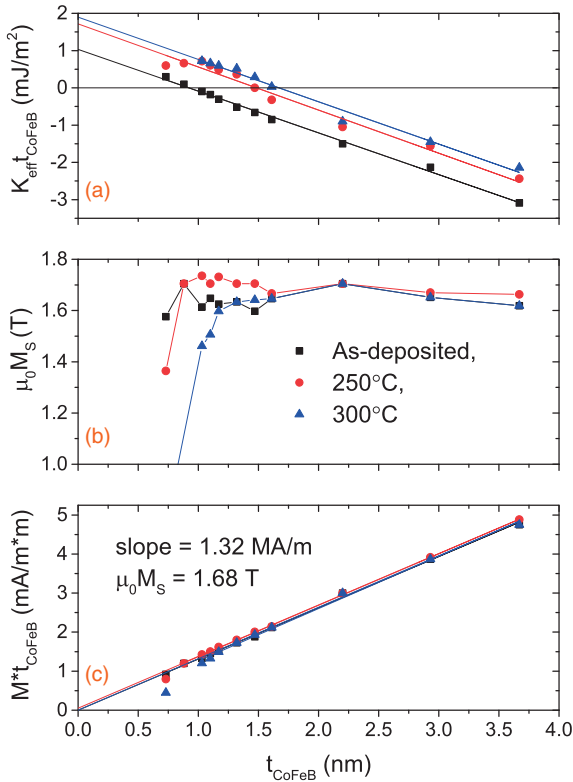


Fig. 1. (a) Product of the effective magnetic anisotropy of the free layer and its thickness t_{CoFeB} as a function of t_{CoFeB} . Linear dependence is maintained down to $t_{\text{CoFeB}} = 1$ nm, below which a deviation is observed, especially after sample annealing. (b) Magnetization saturation values oscillates around $\mu_0 M_s = 1.65$ T. (c) Product of the magnetization on the free layer thickness vs t_{CoFeB} , from which the magnetic dead layer was calculated to be negligible.

effective anisotropy energy density K_{eff} (defined as $K_{\text{eff}} = H_k \times M_s/2$, where H_k is the anisotropy field measured using the VSM along the hard magnetization axis) changes linearly with t_{CoFeB} , as shown in Fig. 1(a), which enables us to calculate the interface anisotropy energy $K_{i,0}$ from the intercept with the y-axis. The same anisotropy values (within an experimental error) are obtained by integrating the area between VSM measurements along the easy and hard axes. $K_{i,0}$ evaluated this way increases from 1 mJ/m^2 for an as-deposited sample to 1.9 mJ/m^2 for a sample after annealing at 300°C , which is higher than that when a Ta buffer is used.^{8,29} We note that this value is comparable to the record high $K_{i,0}$ value reported in³⁰ for MBE-deposited Cr/Fe/MgO.

Next, we discuss the effective thickness of the thin CoFeB layer deposited on the Ir buffer. Deposition of a heavy metal onto a ferromagnet (or vice versa) commonly reduces its effective thickness because of material mixing at the interface. This magnetic dead layer can thus decrease the saturation magnetization and, as a result, change the effective anisotropy of the thin magnetic film.²⁹ To estimate the magnetic dead layer thickness, we calculated the product of M_s and t_{CoFeB} as a function of t_{CoFeB} , as shown in Fig. 1(c). In the as-deposited sample, practically no magnetically dead layer was measured, as the linear fit to the experimental points crosses the $M_s = 0$ axis at $t_{\text{CoFeB}} = 0.1 \text{ \AA}$. After annealing at 250 and 300°C , a deviation from linear behavior

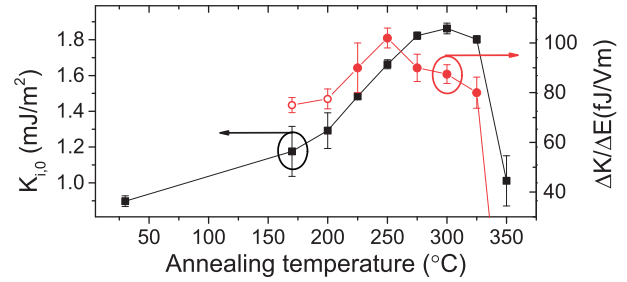


Fig. 2. Interface anisotropy energy K_i and anisotropy change per applied electric field $\Delta K/\Delta E$ as a function of annealing temperature of MTJ with $t_{\text{CoFeB}} = 1.32$ nm. ΔK_i for temperatures below 225°C (open circles) were obtained for the device with $t_{\text{CoFeB}} = 0.88$ nm.

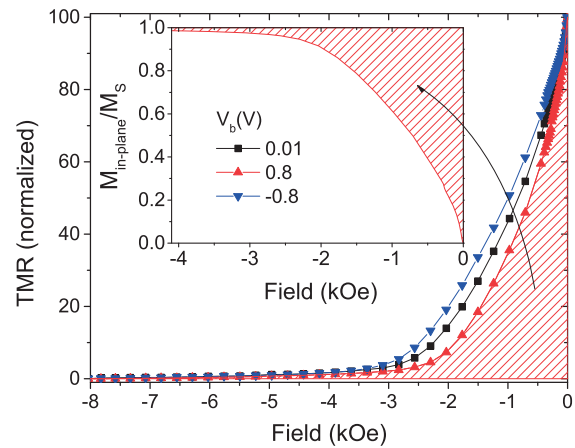


Fig. 3. Normalized TMR vs in-plane field at different bias voltages for the sample annealed at 250°C . PMA energy is calculated from the marked area; an example for $V_b = 0.8$ V is presented in the inset.

can be observed for t_{CoFeB} below 1 nm, which can be explained by interdiffusion of CoFeB and Ir at the interface or by a reduction of the Curie temperature of an ultrathin CoFeB layer.³¹ This feature is also reflected in a drop in M_s in this thickness range. We therefore limit the CoFeB thickness in further studies to the region between 1 nm (linear dependence of $M_s t_{\text{CoFeB}}$ vs t_{CoFeB}) and 1.5 nm (transition to effective in-plane anisotropy). A detailed analysis of the PMA energy versus the annealing temperature in the MTJ with $t_{\text{CoFeB}} = 1.32$ nm is presented in Fig. 2, together with its dependence on the bias voltage (see below).

Having established an optimal CoFeB thickness, we now focus on the transport measurement. Figure 3 presents an example of a TMR curve for an MTJ with $t_{\text{CoFeB}} = 1.32$ nm annealed at 250°C . In the as-deposited state, an in-plane effective anisotropy is measured, which changes to the perpendicular direction upon annealing at 225°C . To extract the PMA energy from the transport measurement, we used the cosine dependence of the MTJ conductance: $G = G_{90} + (G_p - G_{90}) \cos \theta$; consequently, we expressed the ratio of the perpendicular magnetization $M_{\text{in-plane}}$ to M_s as

$$\frac{M_{\text{in-plane}}}{M_s} = \frac{R_{90} - R}{R} \frac{R_p}{R_{90} - R_p}, \quad (1)$$

where R_p (G_p) is the MTJ resistance (conductance) in the parallel state, which is measured in the saturation field; R_{90} (G_{90}) is the MTJ resistance (conductance) in the state of

orthogonal CoFeB layer magnetization orientation, which is measured in zero external magnetic field; and R (G) is the resistance (conductance) in a given in-plane magnetic field. The PMA energy density is calculated by integrating the $M_{\text{in-plane}}(H)$ area; see the example in the inset of Fig. 3. The result agrees well (within an experimental error of 15%) with the anisotropy values obtained from the VSM on unpatterned samples. Then, the TMR versus H curve was measured at different bias voltages (V_b) separated by 0.1 V intervals, and the change in the PMA per applied electric field, $\Delta K/\Delta E$, was derived. For annealing temperatures below 225 °C, where the in-plane magnetization is measured, the $\Delta K/\Delta E$ values were obtained from the MTJ with $t_{\text{CoFeB}} = 0.88$ nm.

The annealing procedure positively affects the MgO/CoFeB interface, which is manifested by an increase in the TMR ratio. Negative TMR, measured at a high negative bias voltage in as-deposited samples (not shown), is not observed after annealing, which also reflects improvement of the interface. Negative TMR can be explained by partial ferromagnet oxidation.³² As expected, the PMA energy also increases with increasing annealing temperature. The effect of the electric field on the PMA also increases after annealing and reaches $\Delta K/\Delta E = 100$ fJ/(V·m) after annealing at 250 °C. Treatment at higher temperatures slightly degrades $\Delta K/\Delta E$, which coincides with saturation of $K_{i,0}$. At annealing temperatures above 325 °C, intermixing between the Ir buffer and CoFeB electrode dramatically increases, which results in a rapid drop in M_s , K_i , and $\Delta K/\Delta E$. Therefore, we conclude that this system is stable only up to 300 °C. We note that $\Delta K/\Delta E$ reaches a maximum value after annealing at lower temperatures than those at which $K_{i,0}$ is maximized, which can be explained by the greater sensitivity of the former to the interface quality. A similar tendency was observed for other buffer materials, which will be discussed elsewhere. Nevertheless, in a single multilayer system, both high PMA and a high anisotropy change under a bias voltage were achieved, which is promising for application.

Recently, a few groups reported a large change in the anisotropy using electric fields;^{33,34} however, in these cases, the anisotropy changes are induced by migration of atoms (oxygen) within the structure, which may limit both the lifetime and operating speed of devices. To demonstrate high-speed operation of our MTJ, we performed high-frequency rectification measurements,³⁵ as shown in Fig. 4. The highest rectification signal was obtained when the magnetic field was applied at 40° from the sample plane, which confirms the dynamics related to the electric-field-induced anisotropy change. The input power from the RF generator was fixed at 0 dBm. In the entire investigated field range, two symmetric peaks are visible in Fig. 4(b). Note that in the magnetic-field-modulation detection method, the derivative of the signal is measured. To understand the origin of these two peaks, we performed macrospin calculations. First, the TMR curve measured in the same geometry was modeled using the cosine behavior of the resistance and relative magnetic moment angle.³⁶ Then, knowing the angle between each ferromagnetic layer moment θ_m and the external magnetic field θ_H with respect to the normal-to-sample plane, we used the following formula to calculate the FMR frequency f :

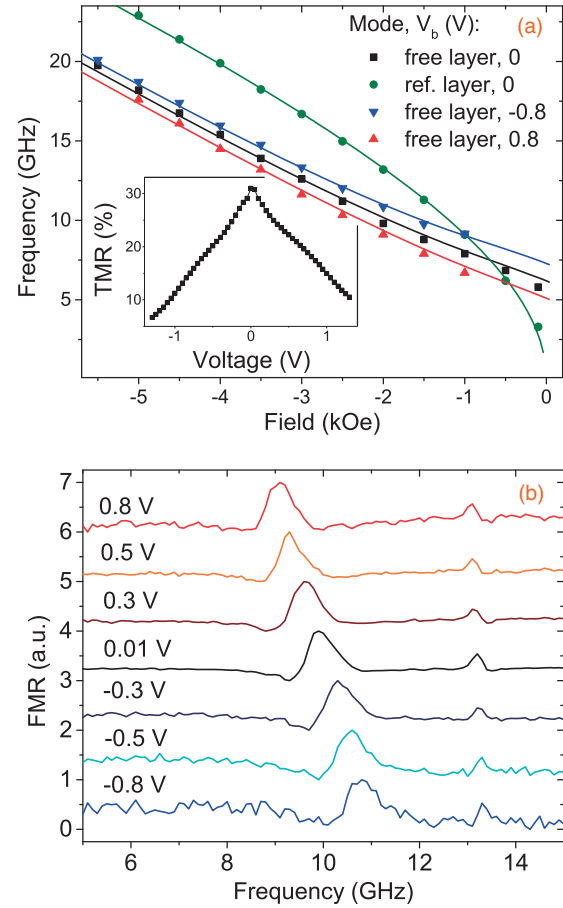


Fig. 4. (a) FMR modes measured in the MTJ annealed at 250 °C with the magnetic field applied at 40° from the sample plane. Solid lines represent solutions to Eq. (2). Change in the oscillation frequency under a bias voltage agrees well with PMA energy change derived from normalized TMR curves. Inset shows bias voltage dependence of the TMR ratio. (b) Bias voltage dependence of the FMR signal measured with $H_{\text{ext}} = -2$ kOe.

$$2\pi f = \gamma \sqrt{H_1 H_2}, \tag{2}$$

$$H_1 = H_{\text{ext}} \cos(\theta_H - \theta_m) + H_{kz} \cos^2(\theta_m),$$

$$H_2 = H_{\text{ext}} \cos(\theta_H - \theta_m) + H_{kz} \cos(2\theta_m),$$

where γ is the gyromagnetic ratio, H_{ext} is the external magnetic field amplitude, and H_{kz} is the effective anisotropy field. For the free layer, $H_{kz} = -H_k$, whereas for the reference layer, H_{kz} equals the demagnetizing field. Thus, by using H_k from the static measurements, we obtained good agreement between the experiment and simulation. In addition, by changing H_k by the amount determined from the bias-voltage-dependent TMR curves, we could model the FMR under a high-bias condition, which also agrees well with FMR data.³⁷

The second peak is very well fitted by the curve that takes only the demagnetizing field into account; thus, we can attribute it to the reference layer dynamics.³⁸ We note that its frequency does not change with the bias voltage.

In conclusion, we presented experimental evidence of high PMA energy in the Ir/CoFeB/MgO trilayer system. In an MTJ structure, we also measured a relatively high electric field effect on the PMA energy, which reaches 100 fJ/(V·m) after the MTJ is annealed at 250 °C; this is essential for a thermally stable and energy-efficient MRAM cell design. We demonstrated a high operating speed of the voltage-

controlled magnetic anisotropy by measuring the rectification signal from a device supplied with an RF signal. We believe that further optimization of heavy metal/ferromagnet/insulator systems will lead to development of a new class of electric-field-controlled magnetic devices.

Acknowledgments We thank E. Usuda, Y. Sato, and M. Sekine for assistance with the experiment and T. Yorozu for a fruitful discussion. This work was partly supported by the Strategic AIST integrated R&D program, “IMPULSE: Initiative for Most Power-efficient Ultra-Large-Scale data Exploration” and the ImPACT Program of the Council for Science, Technology and Innovation (Cabinet Office, Government of Japan). W.S. acknowledges a Foundation for Polish Science (FNP) scholarship under the START Programme.

- 1) Y. Fujisaki, *Jpn. J. Appl. Phys.* **52**, 040001 (2013).
- 2) S. Mangin, D. Ravelosona, J. A. Katine, M. J. Carey, B. D. Terris, and E. E. Fullerton, *Nat. Mater.* **5**, 210 (2006).
- 3) H. Yoda, T. Kishi, T. Nagase, M. Yoshikawa, K. Nishiyama, E. Kitagawa, T. Daibou, M. Amano, N. Shimomura, S. Takahashi, T. Kai, M. Nakayama, H. Aikawa, S. Ikegawa, M. Nagamine, J. Ozeki, S. Mizukami, M. Oogane, Y. Ando, S. Yuasa, K. Yakushiji, H. Kubota, Y. Suzuki, Y. Nakatani, T. Miyazaki, and K. Ando, *Curr. Appl. Phys.* **10**, e87 (2010).
- 4) M. Nakayama, T. Kai, N. Shimomura, M. Amano, E. Kitagawa, T. Nagase, M. Yoshikawa, T. Kishi, S. Ikegawa, and H. Yoda, *J. Appl. Phys.* **103**, 07A710 (2008).
- 5) P. F. Carcia, A. D. Meinhardt, and A. Suna, *Appl. Phys. Lett.* **47**, 178 (1985).
- 6) T. Shinjo, S. Hine, and T. Takada, *J. Phys. Colloq.* **40**, C2-86 (1979).
- 7) S. Yakata, H. Kubota, Y. Suzuki, K. Yakushiji, A. Fukushima, S. Yuasa, and K. Ando, *J. Appl. Phys.* **105**, 07D131 (2009).
- 8) S. Ikeda, K. Miura, H. Yamamoto, K. Mizunuma, H. D. Gan, M. Endo, S. Kanai, J. Hayakawa, F. Matsukura, and H. Ohno, *Nat. Mater.* **9**, 721 (2010).
- 9) T.-I. Cheng, C.-W. Cheng, and G. Chern, *J. Appl. Phys.* **112**, 033910 (2012).
- 10) B. Cui, C. Song, G. Wang, Y. Wang, F. Zeng, and F. Pan, *J. Alloys Compd.* **559**, 112 (2013).
- 11) Q. L. Ma, S. Iihama, T. Kubota, X. M. Zhang, S. Mizukami, Y. Ando, and T. Miyazaki, *Appl. Phys. Lett.* **101**, 122414 (2012).
- 12) Y.-W. Oh, K.-D. Lee, J.-R. Jeong, and B.-G. Park, *J. Appl. Phys.* **115**, 17C724 (2014).
- 13) M. Yamanouchi, R. Koizumi, S. Ikeda, H. Sato, K. Mizunuma, K. Miura, H. D. Gan, F. Matsukura, and H. Ohno, *J. Appl. Phys.* **109**, 07C712 (2011).
- 14) T. Liu, J. W. Cai, and L. Sun, *AIP Adv.* **2**, 032151 (2012).
- 15) D. C. Worledge, G. Hu, D. W. Abraham, P. L. Trouilloud, and S. Brown, *J. Appl. Phys.* **115**, 172601 (2014).
- 16) M. Weisheit, S. Fahler, A. Marty, Y. Souche, C. Poinignon, and D. Givord, *Science* **315**, 349 (2007).
- 17) T. Maruyama, Y. Shiota, T. Nozaki, K. Ohta, N. Toda, M. Mizuguchi, A. A. Tulapurkar, T. Shinjo, M. Shiraishi, S. Mizukami, Y. Ando, and Y. Suzuki, *Nat. Nanotechnol.* **4**, 158 (2009).
- 18) T. Nozaki, Y. Shiota, M. Shiraishi, T. Shinjo, and Y. Suzuki, *Appl. Phys. Lett.* **96**, 022506 (2010).
- 19) S. Yuasa, A. Fukushima, K. Yakushiji, T. Nozaki, M. Konoto, H. Maehara, H. Kubota, T. Taniguchi, H. Arai, H. Imamura, K. Ando, Y. Shiota, F. Bonell, Y. Suzuki, N. Shimomura, E. Kitagawa, J. Ito, S. Fujita, K. Abe, K. Nomura, H. Noguchi, and H. Yoda, *IEDM Tech. Dig.*, 2013, 3-1.
- 20) H. Kubota, S. Ishibashi, T. Saruya, T. Nozaki, A. Fukushima, K. Yakushiji, K. Ando, Y. Suzuki, and S. Yuasa, *J. Appl. Phys.* **111**, 07C723 (2012).
- 21) H. Sato, M. Yamanouchi, S. Ikeda, S. Fukami, F. Matsukura, and H. Ohno, *Appl. Phys. Lett.* **101**, 022414 (2012).
- 22) D. Odkhuu, S. H. Rhim, N. Park, and S. C. Hong, *Phys. Rev. B* **88**, 184405 (2013).
- 23) Y. Miura, M. Tsujikawa, and M. Shirai, *J. Appl. Phys.* **113**, 233908 (2013).
- 24) J. W. Koo, S. Mitani, T. T. Sasaki, H. Sukegawa, Z. C. Wen, T. Ohkubo, T. Niizeki, K. Inomata, and K. Hono, *Appl. Phys. Lett.* **103**, 192401 (2013).
- 25) A. Koziol-Rachwał, W. Skowroński, T. Ślęzak, D. Wilgocka-Ślęzak, J. Przewoźnik, T. Stobiecki, Q. H. Qin, S. van Dijken, and J. Korecki, *J. Appl. Phys.* **114**, 224307 (2013).
- 26) C.-H. Lambert, A. Rajanikanth, T. Hauet, S. Mangin, E. E. Fullerton, and S. Andrieu, *Appl. Phys. Lett.* **102**, 122410 (2013).
- 27) Y. Shiota, S. Murakami, F. Bonell, T. Nozaki, T. Shinjo, and Y. Suzuki, *Appl. Phys. Express* **4**, 043005 (2011).
- 28) A. M. Gonçalves, I. Barsukov, Y.-J. Chen, L. Yang, J. A. Katine, and I. N. Krivorotov, *Appl. Phys. Lett.* **103**, 172406 (2013).
- 29) J. Sinha, M. Hayashi, A. J. Kellock, S. Fukami, M. Yamanouchi, H. Sato, S. Ikeda, S. Mitani, S.-h. Yang, S. S. P. Parkin, and H. Ohno, *Appl. Phys. Lett.* **102**, 242405 (2013).
- 30) J. Okabayashi, J. W. Koo, H. Sukegawa, S. Mitani, Y. Takagi, and T. Yokoyama, *Appl. Phys. Lett.* **105**, 122408 (2014).
- 31) R. Zhang and R. F. Willis, *Phys. Rev. Lett.* **86**, 2665 (2001).
- 32) C. Tiusan, J. Faure-Vincent, C. Bellouard, M. Hehn, E. Jouguelet, and A. Schuhl, *Phys. Rev. Lett.* **93**, 106602 (2004).
- 33) A. Rajanikanth, T. Hauet, F. Montaigne, S. Mangin, and S. Andrieu, *Appl. Phys. Lett.* **103**, 062402 (2013).
- 34) U. Bauer, S. Emori, and G. S. D. Beach, *Appl. Phys. Lett.* **100**, 192408 (2012).
- 35) T. Nozaki, Y. Shiota, S. Miwa, S. Murakami, F. Bonell, S. Ishibashi, H. Kubota, K. Yakushiji, T. Saruya, A. Fukushima, S. Yuasa, T. Shinjo, and Y. Suzuki, *Nat. Phys.* **8**, 492 (2012).
- 36) W. Skowroński, M. Czapkiewicz, M. Frankowski, J. Wrona, T. Stobiecki, G. Reiss, K. Chalapat, G. S. Paraoanu, and S. van Dijken, *Phys. Rev. B* **87**, 094419 (2013).
- 37) W. Skowroński, M. Frankowski, J. Wrona, T. Stobiecki, P. Ogrodnik, and J. Barnaś, *Appl. Phys. Lett.* **105**, 072409 (2014).
- 38) In the calculations, we used the following data: $\gamma = 2.9$ GHz/T, $\theta_H = 50^\circ$, $H_k = 1.75, 2.125, \text{ and } 2.5$ kOe for a bias voltage V_b equal to $+0.8, 0.01, \text{ and } -0.8$, respectively, and a demagnetizing field of the reference layer $H_{\text{demag}} = 12$ kOe.